Magnetic flux quanta in annular Josephson junctions in a barrier-parallel dc magnetic field

S. Keil, I. V. Vernik,* T. Doderer, A. Laub, H. Preβler, and R. P. Huebener
Physikalisches Institut, Lehrstuhl Experimentalphysik II, Universität Tübingen, Auf der Morgenstelle 14, D-72076 Tübingen, Germany

N. Thyssen, A. V. Ustinov, and H. Kohlstedt
Institut für Schicht- und Ionentechnik, Forschungszentrum Jülich (KFA), D-52425 Jülich, Germany

(Received 1 April 1996; revised manuscript received 6 August 1996)

Flux quanta (fluxons) trapped in an annular Josephson junction reside in a spatially periodic pinning potential when a uniform external magnetic field is applied parallel to the plane of the junction's tunnel barrier. We investigate the fluxon behavior by measuring the current versus voltage curves, the magnetic dependence of the junction critical current, and by means of spatially resolved measurements imaging the pinned fluxons. We derive the fluxon potential energy including fluxon-fluxon interaction. Fair agreement of this calculation with our experimental results is obtained. [S0163-1829(96)03846-5]

Fluxoid quantization in a superconducting ring is one of the most striking properties of superconductors being macroscopic quantum systems where the quantum mechanical wave function, describing the Cooper pairs, must be single valued (see, e.g., Ref. 1). Recently, annular Josephson junctions, consisting of two superconducting rings which are coupled by a thin dielectric tunneling barrier, were the subject of increasing interest.[2–7] If each of the two superconducting junction electrodes is thicker than the magnetic penetration depth λ_L (which is the case for the samples studied here), the total magnetic flux in the annular junction is conserved. The flux quantum $\Phi_0 = h/2e$ in the junction is called Josephson vortex or fluxon and its behavior is accurately described by the perturbed sine-Gordon equation[8] (h is Planck's constant and e the elementary charge). The pure sine-Gordon equation, which neglects dissipative motion of the fluxons, has solitonic solutions which correspond to the fluxons in real junctions in the limit of small perturbations. The motivation to study annular Josephson junctions comes mainly from the solitonic properties of fluxons moving in the junction without an influence of boundaries and from the conservation of the algebraic sum of the fluxon number.

In this paper we show experimental results dealing with fluxons in an annular Josephson junction located in a dc magnetic field **B** applied parallel to the plane of the junction tunneling barrier and parallel to the current leads [see the inset of Fig. 1(a)]. The trapped fluxons then reside in a spatially periodic pinning potential[3,4]

$$U_p = -\mathbf{m}\cdot\mathbf{B} = -|\mathbf{m}||\mathbf{B}|\cos\frac{2\pi x}{l} \tag{1}$$

with the period equal to the circumference of the junction. Here, **m** is the magnetic moment of the fluxon, x is the coordinate running azimuthally around the junction starting at the minimum of U_p, and l is the junction circumference. The height of the potential well, being proportional to B ($B = |\mathbf{B}|$), can easily be controlled during our measurements. The sample geometry can be found in the inset of Fig. 1(a). The following results were obtained with a Nb/AlO_x/Nb junction having a critical current density $j_c = 60$ A/cm^2 at 4.2 K, an inner ring radius $r_i = 61\ \mu$m, and a ring width $w = 10\ \mu$m. The Josephson penetration depth λ_J is 50 μm, thus, the normalized junction length $L = 2\pi(r_i + w/2)/\lambda_J = 8.3$. Since $w \ll \lambda_J$ we are dealing with a one-dimensional annular junction and, in the following, we will neglect any spatial dependence in radial direction.

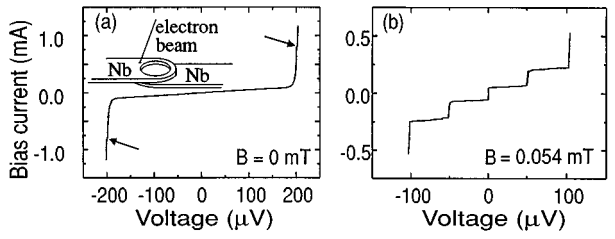

FIG. 1. Current-voltage characteristics of the annular Josephson junction with four trapped fluxons (a) without applied magnetic field and (b) with magnetic field ($T = 4.2$ K). The inset shows a sketch of our samples.

Figure 1 shows current versus voltage curves (IVC's) obtained for the case of four trapped fluxons without and with applied magnetic field. Fluxon trapping can easily be obtained by cooling the sample through the superconducting transition temperature while some current is passing through the junction. After fluxon trapping, we checked the IVC and only in the case of nearly vanishing critical current I_c [as shown in Fig. 1(a)], indicating conditions where only trapped fluxons are present without additional trapped flux in the superconducting environment, we continued our measurements.

The IVC without applied magnetic field is shown in Fig. 1(a). In this case there are four traveling fluxons in the junction. We note that by careful inspection of the current steps at $\pm$ 200 μ V one observes a small shift of the voltage towards higher values at about 0.8 mA (indicated by the arrows) due to fluxon bunching.[5] When B is increased, I_c increases also due to fluxon pinning in the periodic potential. In addition, the step near $\pm$ 200μ V observed without **B** vanishes and the third fluxon step appears indicating that there are three fluxons traveling in the junction while one fluxon is

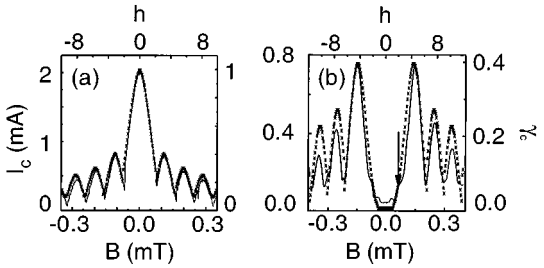

FIG. 2. Magnetic interference patterns I_c vs B. The points represent the numerical data, the solid lines show the experimental results (a) without trapped fluxons, (b) with four trapped fluxons. The arrow marks the magnetic field used for obtaining Fig. 3(b) ($T=4.2$ K).

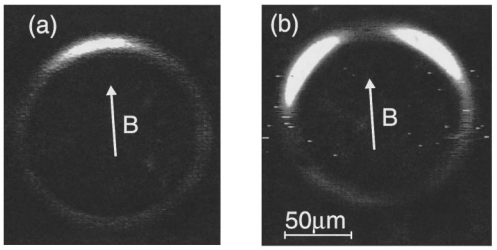

FIG. 3. Voltage images $-\Delta V(x_0)$ of the annular junction ($T=4.5$ K). (a) Two fluxons are trapped and one of them is pinned, $B=0.05$ mT. (b) Four fluxons are trapped and two of them are pinned, $B=0.07$ mT. Bright areas indicate the collision sites where the moving fluxons collide with the pinned ones. The orientation of **B** is indicated.

pinned. Figure 1(b) shows the situation when there are two fluxons pinned out of the four trapped fluxons. In addition to the second step at approximately $\pm 100\ \mu$V, for smaller bias currents there is the first step indicating three pinned fluxons for this smaller driving force.

Martucciello and Monaco calculated analytically the magnetic diffraction pattern I_c vs B for annular junctions in case of N trapped fluxons and small one-dimensional junctions (i.e., $2\pi(r_i+w/2)<\lambda_J$ and $w\ll\lambda_J$). They show that I_c modulates according to the Bessel function of order N of the magnetic field.[9] Figure 2 shows our measured data in case of $N=0$ and $N=4$. We measured I_c vs B for $N\leqslant 8$. In order to investigate numerically the dependence I_c vs B we used the pertubed sine-Gordon model approach suggested by Grønbech-Jensen *et al.*:[3,4]

$$\Phi_{\xi\xi}-\Phi_{\tau\tau}=\sin\Phi+\alpha\Phi_{\tau}-\gamma-h\sin\frac{2\pi\xi}{L}, \qquad (2)$$

where Φ is the phase difference between the two macroscopic wave functions of the junction electrodes. The spatial coordinate ξ is normalized to λ_J, the time τ is normalized to the inverse plasma frequency ω_0^{-1}, α is the dissipation coefficient due to the quasiparticle tunneling through the tunnel barrier, and γ is the bias current density normalized to the critical current density j_c of the junction. The last term in Eq. (2) accounts for the applied barrier-parallel magnetic field whose dimensionless amplitude $h\sim H$ is normalized by a sample-specific geometrical factor.[3,4,7] Equation (2) is accompanied by the periodic boundary conditions:

$$\Phi(L)=\Phi(0)+N2\pi;\Phi_{\xi}(L)=\Phi_{\xi}(0), \qquad (3)$$

which assume that there are N fluxons trapped. To calculate the critical current of the junction we used a straightforward way of integrating Eq. (2) numerically with the boundary conditions Eq. (3). Figure 2 shows fair agreement of the numerically calculated data with the measured curves for the examples $N=0$ and $N=4$.

Our results show that the field value up to which $I_c\approx 0$ increases with N. Such a behavior can qualitatively be explained by the mutual interaction of the unipolar fluxons trapped in the junction and their interaction with **B**. If $N=1$, the single fluxon will be located in the potential minimum, i.e., the magnetic moment **m** of the fluxon will be parallel to **B**. If $N\geqslant 2$, the fluxon lattice is arranged symmetrical on both sides with respect to the coordinate $x=0$. However, for the same B the pinning strength per fluxon is obviously smaller than in the case of $N=1$ due to the variation of the pinning potential according to Eq. (1) and the impossibility to have more than one flux quantum residing at the $x=0$ location.

We performed spatially resolved measurements by means of low-temperature scanning electron microscopy (LTSEM).[10,11] LTSEM allows the local thermal perturbation of the junction due to the electron beam with the focus at x_0 during operation of the sample at liquid-helium temperatures. The spatial extension of the perturbation is given by the thermal healing length and this value determines the spatial resolution, being about 1–2 μm for the samples studied here. The temperature increment $\Delta T(x_0)$ can be tuned by the electron-beam power, and is adjusted to about 1–3 K for the present studies. Since the thermal relaxation time for the beam-induced local thermal perturbation is about 100 ns, the sample response signal is a time-averaged information about the junction dynamics. The latter evolves on a time scale of about 10 ps.

In this article we present two different imaging techniques for the pinned fluxons. The first method uses the electron-beam-induced additional energy loss during the collision of two fluxons. In case of fluxon-antifluxon collisions, we have observed a significant electron-beam-induced voltage signal $\Delta V(x_0)<0$ of the current-biased junction at the collision sites.[6,12] Notice, here we are dealing with the collision of unipolar fluxons in contrast to the fluxon-antifluxon collisions considered in Refs. 6 and 12. Our experimental results show that also in the case of the collision of unipolar fluxons, the local thermal perturbation due the electron beam causes a significant sample response $\Delta V(x_0)<0$ at the collision sites.

Collisions are expected for the situation shown in Fig. 1(b) where four fluxons are trapped in the junction, while two of them are moving and two are pinned by the applied magnetic field if the junction is biased on the step at about 100 μV. Figure 3(b) shows the LTSEM image of this situation. The two pinned fluxons are clearly visible in form of the two bright regions. In Fig. 3(a) we show the collision image of a single pinned fluxon when two fluxons are trapped in the junction. Here, the pinned fluxon is located close to the minimum of U_p with **m** parallel to **B** [see Eq. (1)]. The moving fluxon is used as a detector for the pinned one by the collision that takes place once during each revo-

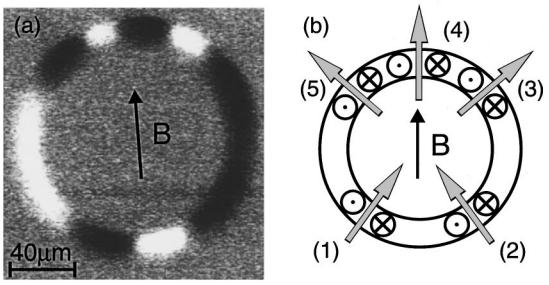

FIG. 4. (a) Electron-beam-induced change of the maximum junction critical current $-\Delta I_c(x_0)$ ($T=4.5$ K). Bright (dark) areas indicate a dc Josephson current flow from bottom to top electrode (from top to bottom electrode). The orientation of **B** is indicated ($B=0.19$ mT). (b) Sketch of the pinned fluxons [gray arrows labeled from (1) to (5)] as inferred from (a). $\odot$ and $\otimes$ indicate the direction of the Josephson current flow.

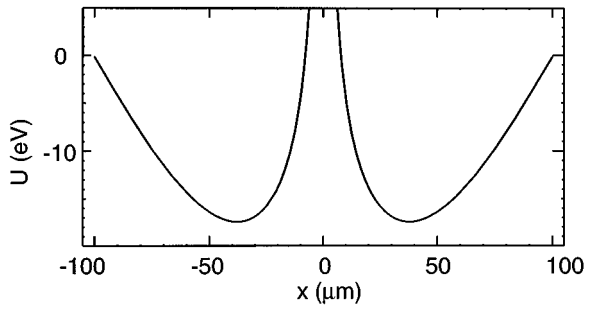

FIG. 5. Calculated total potential energy U from Eq. (5) using the symmetric fluxon configuration with respect to $x=0$ and assuming $B=0.19$ mT for the case of the fluxons (1) and (2) in Fig. 4.

lution of the moving fluxon. Our collision images show a small deflection (in counter-clockwise direction) of the pinned fluxons from the potential minimum due to the impact during the collision.

The use of the second method results in the two-dimensional imaging of the spatial distribution of the maximum dc Josephson current density[13,14]

$$J(x)=j_c(x)\sin\Phi(x) \tag{4}$$

depending on j_c and on the phase difference Φ. In our case, where j_c does not show any significant spatial dependence across the junction,[15] $J(x)$ is directly proportional to $\sin\Phi(x)$. The local thermal perturbation induced by the electron beam at x_0 decreases $j_c(x_0)$ and, neglecting any nonlocal effect, the change $\Delta J(x_0)$ is a direct measure of $\sin\Phi(x_0)$.[13] The total critical current of the junction

$$I_c=\int_0^l j_c\sin\Phi(x)dx \tag{5}$$

is continuously measured during scanning the e beam across the sample and we obtain the data

$$-\Delta I_c(x_0)\propto\sin\Phi(x_0) \tag{6}$$

if the area perturbed by the beam is small compared to λ_J. In case of a hysteretic IVC [e.g., at the maxima of the $I_c(B)$] this imaging technique is described in Ref. 13, whereas for a nonhysteretic IVC [e.g., at the minima of the $I_c(B)$] a description of the imaging technique can be found in Ref. 14. For all bias conditions where $dI_c/dB=0$ nonlocal effects of the local perturbation due to the macroscopic quantum properties of a Josephson junction can be ruled out[16] and all images shown in this paper are obtained under this condition.

Figure 4 shows the image when one trapped fluxon is pinned and the magnetic field is adjusted to a higher value such that there is significant penetration of flux and antiflux into the junction. For the magnetic-field value used for this image [at a minimum of $I_c(B)$], approximately two fluxons and two antifluxons penetrate the junction in addition to the single trapped fluxon. (Notice, only the total amount of flux in the junction is conserved and not the flux or antiflux independently.) This image in part (a) shows the spatial distribution of the maximum dc Josephson tunneling current according to Eq. (6). From this we deduce a fluxon lattice as depicted in Fig. 4(b).

The current images $-\Delta I_c(x_0)$ described above directly show the spatial distribution of $\sin\Phi(x)$ and, hence, we obtain $\Phi(x)$ modulo 2π. The collision images (Fig. 3) directly yield the location of the pinned fluxons, being described by the maximum of the derivative $d\Phi/dx$.

The total potential energy U of one fluxon for the case of two pinned fluxons can be calculated to be

$$U(x)=U_p(x)+U_r(x)+U_i(x). \tag{7}$$

For this calculation we use the symmetry of the two-fluxon lattice with respect to $x=0$. U_p is found from Eq. (1)

$$U_p(x)=-\frac{3}{2\mu_0}\Phi_0 wB\cos\frac{2\pi x}{l}. \tag{8}$$

μ_0 is the permeability of free space. The repulsion of unipolar fluxons results in Ref. 17

$$U_r(x)=4\Phi_0 j_c\lambda_J w\exp\left(-\frac{2|x|}{\lambda_J}\right). \tag{9}$$

Equation (9) is only correct for a distance $D=2|x|$ between the two fluxons larger than λ_J and results from the overlapping of the two fluxons. Due to the symmetry of the fluxon lattice one fluxon is located at x and the other one at $-x$ such that the distance between them is $2|x|$. In case that the fluxons are closely spaced and softly compressed in the pinning potential, another contribution to the total energy becomes important, namely the inner fluxon energy

$$U_i(x)=\frac{w\Phi_0^2}{\pi^2\mu_0 d|x|}, \tag{10}$$

becoming most relevant for the distance $D=2|x|<2\lambda_J$. $d=2\lambda_L+d_I$ with d_I being the thickness of the dielectric tunneling barrier. The function $U_i(x)$ is calculated by introducing the pure soliton solution

$$\Phi(\xi)=4\arctan\{\exp(\xi-\xi_c)\} \tag{11}$$

of the sine-Gordon equation into the static sine-Gordon Hamiltonian[8]

$$H=\int_0^L\left\{\frac{1}{2}\left(\frac{\partial\Phi}{\partial\xi}\right)^2+1-\cos\Phi\right\}d\xi. \tag{12}$$

ξ_c denotes the center of mass of the fluxon. To obtain Eq. (10), we introduced the soft fluxon compression in form of a perturbation treatment by the assumption that λ_J, being a measure of the length of the free fluxon, is replaced by the distance $D=2|x|$ for closely spaced fluxons. This assumption is justified by the agreement of the calculation with our experimental results.

Figure 5 shows $U(x)$ calculated for the situation of Fig. 4 in the lower half of the junction [fluxon (1) and (2) in Fig. 4(b)]. The distance D between the two pinned fluxons is assumed to be the distance between the two minima of $U(x)$. From Fig. 5 we obtain $D=76\ \mu$m, in agreement with the experimental result shown in Fig. 4(a). The same calculation applied for the situation of Fig. 3(b) results in $D=110\ \mu$m, whereas the experiment indicates $D=106\ \mu$m. Finally, we calculated $U(x)$ for the case of three fluxons as observed in the upper half of Fig. 4(a) [fluxons (3), (4), and (5) in Fig. 4(b)] by using the symmetry of the fluxon lattice with respect to $x=0$. The calculation yields $51\ \mu$m for the distance between two adjacent fluxons, whereas in the experiment we measure $60\ \mu$m. For the calculation we consider the repulsion between the next-nearest-neighbor fluxon (3) and (5) but not the attraction between the fluxons (1) and (5) or (2) and (3). This may explain that the measured distance is slightly larger than the calculated one.

Finally, we note that the fluxon potential energy Eq. (7) (see Fig. 5) resembles that of atoms in a crystal lattice. An expansion of the fluxon lattice is expected due to the anharmonicity of U, if the fluxon energy is increased similar to the thermal expansion of a crystal lattice.

We are grateful to J. Powileit for providing us with a sample probe. We thank N. Martucciello and R. Monaco for sharing their results with us before publication. I.V.V. wants to thank the Deutscher Akademischer Austauschdienst for financial support.

*Permanent address: Institute of Solid State Physics, Russian Academy of Sciences, Chernogolovka 142432, Russia.

[1] M. Tinkham, *Introduction to Superconductivity*, 2nd ed. (McGraw-Hill, New York, 1996).
[2] A. Davidson, B. Dueholm, B. Kryger, and N.F. Pedersen, Phys. Rev. Lett. **55**, 2059 (1985).
[3] N. Grønbech-Jensen, P.S. Lomdahl, and M.R. Samuelsen, Phys. Lett. A **154**, 14 (1991).
[4] N. Grønbech-Jensen, P.S. Lomdahl, and M.R. Samuelsen, Phys. Rev. B **43**, 12 799 (1991).
[5] A.V. Ustinov, T. Doderer, R.P. Huebener, N. F. Pedersen, B. Mayer, and V.A. Oboznov, Phys. Rev. Lett. **69**, 1815 (1992).
[6] A. Laub, T. Doderer, S.G. Lachenmann, R.P. Huebener, and V.A. Oboznov, Phys. Rev. Lett. **75**, 1372 (1995).
[7] N. Martucciello and R. Monaco, Phys. Rev. B **53**, 3471 (1996).
[8] D.W. McLaughlin and A.C. Scott, Phys. Rev. A **18**, 1652 (1978).
[9] N. Martucciello and R. Monaco (unpublished).
[10] R.P. Huebener, in *Advances in Electronics and Electron Physics*, edited by P.W. Hawkes (Academic, New York, 1988), Vol. 70, p. 1.
[11] R. Gross and D. Koelle, Rep. Prog. Phys. **57**, 651 (1994).
[12] S.G. Lachenmann, G. Filatrella, A.V. Ustinov, T. Doderer, N. Kirchmann, D. Quenter, J. Niemeyer, and R. Pöpel, J. Appl. Phys. **77**, 2598 (1995).
[13] J. Bosch, R. Gross, M. Koyanagi, and R.P. Huebener, Phys. Rev. Lett. **54**, 1448 (1985); J. Low Temp. Phys. **68**, 245 (1987).
[14] D. Quenter, A.V. Ustinov, S.G. Lachenmann, T. Doderer, R.P. Huebener, F. Müller, J. Niemeyer, R. Pöpel, and T. Weimann, Phys. Rev. B **51**, 6542 (1995)
[15] This can easily be checked by measuring the spatial distribution of the quasiparticle tunneling current density across the junction; (see, e.g., Refs. 5, 10, and 11).
[16] J.-J. Chang, C.H. Ho, and D.J. Scalapino, Phys. Rev. B **31**, 5826 (1985).
[17] K.K. Likharev, *Dynamics of Josephson Junctions and Circuits* (Gordon and Breach, New York, 1986), Sec. 15.2.